A p-version MITC finite element method for Reissner-Mindlin plates with curved boundaries ⋆

Christos Xenophontos [a,*] , Jason Kurtz [b] and Scott Fulton [c]

[a] *Department of Mathematical Sciences, Loyola College, 4501 N. Charles Street, Baltimore, MD 21210-2699.*

[b] *Texas Institute for Computational and Applied Mathematics, Applied Computational and Engineering Science Building, Austin, TX 78712-1085.*

[c] *Division of Mathematics and Computer Science, Clarkson University, Potsdam NY 13699-5815.*

This article is dedicated to the memory of George Mackiw

Abstract

We consider the approximation of Reissner-Mindlin plates with curved boundaries, using a p-version MITC finite element method. We describe in detail the formulation and implementation of the method, and emphasize the need of a Piola-type map in order to handle the curved geometry of the elements. The results of our numerical computations demonstrate the robustness of the method and suggest that it gives near exponential convergence when the error is measured in the energy norm. For the robust computation of quantities of engineering interest, such as the shear force, the proposed method yields very satisfactory results without the need for any additional post-processing. Comparisons are made with the standard formulation, with and without post-processing.

Key words: Reissner-Mindlin plate, p-version, MITC elements, shear locking, curved elements
PACS: 02.60.Lj, 02.70.Dh, 02.70.-c, 02.60.Cb, 02.60.-x

⋆ Technical Report 2003-03, Department of Mathematical Sciences, Loyola College, 4501 N. Charles Street, Baltimore, MD 21210.

* Corresponding author.
Email addresses: cxenophontos@loyola.edu (Christos Xenophontos), kurtzj@ices.utexas.edu (Jason Kurtz), fulton@clarkson.edu (Scott Fulton).

1 Introduction

The Reissner-Mindlin (R-M) plate model is a widely used system of partial differential equations which describes the deformation of a thin plate subject to transverse loading. This two-dimensional model often replaces the full three-dimensional elasticity problem, when the thickness of the plate is small.

The numerical approximation of the solution to the R-M plate model has received much attention in recent years. Several techniques have been proposed to alleviate the two major computational difficulties associated with this problem, namely the presence of *locking* and *boundary layer* effects. The former occurs due to the inability of the approximating spaces to satisfy certain constraints imposed on the solution as the thickness t of the plate tends to zero. The latter is due to the fact that the system of partial differential equations that describes the R-M plate model is singularly perturbed. The interplay of both phenomena is a rather complicated affair and the question of how to alleviate them *both* is still a mathematically open question (cf. [21]). Nevertheless, if one "separates" the two phenomena, then it is possible to design methods that yield very satisfactory results [13]. To deal with locking, there are two approaches one can take in the context of the Finite Element Method (FEM): (i) enforce Kirchhoff's constraint exactly (by using, e.g., the high-order p/hp versions of the FEM), or (ii) enforce Kirchhoff's constraint *weakly*, by using a modified variational formulation. To deal with boundary layers, the mesh has to be properly designed and in particular it should contain *thin* (anisotropic) elements along the boundary. If the proper mesh design is combined with the p/hp version of the FEM, then exponential rates of convergence are possible.

Our goal in this article is to combine the above approaches, namely the p/hp version of the FEM with a modified formulation, and extend their applicability to R-M plates with curved boundaries. In particular, we consider the so-called *Mixed Interpolated Tensorial Components* (MITC) elements, originally introduced in [6] in terms of the h version of the FEM, and extended and analyzed in [18] in terms of the hp version. Even though in [18] the hp MITC method was defined for general curvilinear domains, the analysis was carried out only for straight-sided elements. Moreover, the only available numerical results showing the robustness of the hp MITC method are found in [28], and once more they are carried out only for straight-sided elements. (See also [29] for more on the approximation theory of hp MITC elements.) We wish to extend the results from [28] to the case of curved elements, and verify that the (original) definition of the hp MITC elements from [18] indeed works in practice when one deals with curvilinear domains. Building on the ideas used for nearly incompressible elasticity in [24], we are able to construct a p version MITC method with the following properties:

- The method performs well, independently of the thickness of plate or the error measure used, provided one uses the proper mesh design for capturing the boundary layer that is (generally) present in the solution.
- No additional post-processing is required for the accurate calculation of quantities of engineering interest.
- Curved elements are handled with the use of a Piola-type mapping.

We hope that the present article will provide the groundwork for future research on these methods, especially in establishing the observed near exponential convergence rates.

In what follows, the usual L^2 inner product and norm are denoted by

$$(f,g)_\Omega = \int_\Omega fg \; dA, \quad \|f\|_{0,\Omega} = \sqrt{(f,f)_\Omega},$$

where $\Omega \subset \mathbb{R}^2$ with boundary $\partial\Omega$ smooth. The usual Sobolev norms

$$\|f\|_{r,\Omega}^2 = \sum_{|\vec{\alpha}|\le r} \left\| \frac{\partial^{|\vec{\alpha}|} f}{\partial x^{\alpha_1} \partial y^{\alpha_2}} \right\|_{0,\Omega}^2,$$

with $\vec{\alpha} = (\alpha_1, \alpha_2) \in \mathbb{N}^2$ a two-index ($|\vec{\alpha}| = \alpha_1 + \alpha_2$), lead naturally to the associated Sobolev spaces

$$H^r(\Omega) = \{f : \|f\|_{r,\Omega} < \infty\}.$$

In particular, the zeroth-order spaces

$$L^2(\Omega) = \{f : \|f\|_{0,\Omega} < \infty\},$$
$$L_0^2(\Omega) = \{f \in L^2(\Omega) : (f,1)_\Omega = 0\},$$

and the first-order spaces

$$H^1(\Omega) = \{f \in L^2(\Omega) : \vec{\nabla} f \in [L^2(\Omega)]^2\},$$
$$H_0^1(\Omega) = \{f \in H^1(\Omega) : f|_{\partial\Omega} = 0\}.$$

play a central role. Finally, the condensed notation,

$$\|(\vec{\phi}, w)\|_{r,s,\Omega}^2 = \|\vec{\phi}\|_{r,\Omega}^2 + \|w\|_{s,\Omega}^2 = \|\phi_1\|_{r,\Omega}^2 + \|\phi_2\|_{r,\Omega}^2 + \|w\|_{s,\Omega}^2$$

defines a norm on the product space $[H^r(\Omega)]^2 \times H^s(\Omega)$.

The rest of the paper is organized as follows: In Section 2 we present the R-M equations and their discretization. Section 3 details the derivation and implementation of a p version MITC method for curved elements and Section 4 contains the results of numerical computations for two model problems. Our conclusions are presented in Section 5.

2 The Reissner-Mindlin plate model and its discretization

Consider the bending of a homogeneous isotropic plate of thickness $t > 0$, occupying the region $\mathcal{R} = \Omega \times (-t/2, t/2)$, where $\Omega \subset \mathbb{R}^2$ represents the midplane of the plate, under normal load density given by $t^3 g(x, y)$, where g is independent of t. The equations of equilibrium for the rotation $\vec{\phi}$, and transverse displacement w are

$$-\frac{D}{2}\left((1-\nu)\vec{\Delta}\vec{\phi} + (1+\nu)\vec{\nabla}\nabla\cdot\vec{\phi}\right) - G\kappa t^{-2}\left(\vec{\nabla}w - \vec{\phi}\right) = \vec{0}, \tag{1}$$

$$-G\kappa t^{-2}\nabla\cdot\left(\vec{\nabla}w - \vec{\phi}\right) = g, \tag{2}$$

where E is Young's modulus, ν is Poisson's ratio, $G = E/2(1+\nu)$ is the elastic shear modulus, $D = E/12(1-\nu^2)$ is the modulus of flexural rigidity, and κ is the shear correction factor (often chosen as $5/6$).

It is well known that the solution to the second-order R-M system (1)–(2) converges to the solution of the fourth-order Biharmonic equation as $t \to 0$, i.e., the solution to the R-M plate satisfies *Kirchhoff's constraint*

$$\vec{\nabla}w - \vec{\phi} = \vec{0}. \tag{3}$$

Practically, this means that straight fibers normal to the undeformed midplane remain straight and normal to the deformed midplane $w(x, y)$. This fact leads to difficulty in approximating the solution to (1)–(2) for very thin plates, because the discretization of the second-order system is being used to approximate functions that are converging to the solution of a fourth-order equation. Our goal is to obtain a discretization of (1)–(2) that performs well independently of t, on a domain with curved boundaries. In practice, one is often interested in the accurate approximation of the stress and moment resultants, such as the shear force

$$\vec{Q} = \langle Q_x,\ Q_y\rangle = -G\kappa t^{-2}(\vec{\nabla}w - \vec{\phi}). \tag{4}$$

Without loss of generality, we will restrict our description of the method to hard clamped plates, where the displacement and rotation are zero on $\partial\Omega$.

Our numerical results in Section 4 ahead, will demonstrate the applicability of the method to other boundary conditions as well. To obtain a variational formulation for the R-M equations, we take the dot product of (1) with a vector test function $\vec{\theta}$, multiply (2) by a scalar test function ζ, integrate over Ω, and add the resulting equations. Assuming the required regularity on all functions involved, we use Green's formula to obtain the standard variational formulation: find $(\vec{\phi}, w) \in [H_0^1(\Omega)]^2 \times H_0^1(\Omega)$ such that

$$\frac{D}{2}a(\vec{\phi},\vec{\theta}) + G\kappa t^{-2}b(\vec{\phi}, w; \vec{\theta}, \zeta) - c(\vec{\phi}, w; \vec{\theta}, \zeta) = \int_\Omega g\zeta \; dA \tag{5}$$

for all $(\vec{\theta}, \zeta) \in [H_0^1(\Omega)]^2 \times H_0^1(\Omega)$, where

$$\begin{aligned} a(\vec{\phi},\vec{\theta}) &= \int_\Omega \Big\{(1-\nu)(\vec{\nabla}\phi_1 \cdot \vec{\nabla}\theta_1 + \vec{\nabla}\phi_2 \cdot \vec{\nabla}\theta_2) \\ &\qquad + (1+\nu)(\nabla \cdot \vec{\phi})(\nabla \cdot \vec{\theta})\Big\}\, dA, \qquad (6) \\ b(\vec{\phi}, w; \vec{\theta}, \zeta) &= \int_\Omega \left(\vec{\nabla}w - \vec{\phi}\right) \cdot \left(\vec{\nabla}\zeta - \vec{\theta}\right) \; dA, \qquad (7) \\ c(\vec{\phi}, w; \vec{\theta}, \zeta) &= \frac{D}{2}\int_{\partial\Omega} \Big\{(1-\nu)(\theta_1\vec{\nabla}\phi_1 + \theta_2\vec{\nabla}\phi_2) + (1+\nu)(\nabla\cdot\vec{\phi})\vec{\theta}\Big\} \cdot \hat{n} ds \\ &\qquad + G\kappa t^{-2}\int_{\partial\Omega} \zeta(\vec{\nabla}w - \vec{\phi}) \cdot \hat{n} ds. \end{aligned}$$

and $\hat{n}$ is the outward unit normal to $\partial\Omega$. Since we are considering only hard clamped plates, the integrals in $c(\vec{\phi}, w; \vec{\theta}, \zeta)$ vanish. For other types of boundary conditions, some or all of these terms are nonzero.

The left hand side of (5) is a continuous and coercive bilinear form, namely there exist positive constants C_1 and C_2 such that

$$\begin{aligned} &\frac{D}{2}a(\vec{\phi},\vec{\theta}) + G\kappa t^{-2}b(\vec{\phi}, w; \vec{\theta}, \zeta) \le C_1 \|(\vec{\phi}, w)\|_{1,1,\Omega} \|(\vec{\theta}, \zeta)\|_{1,1,\Omega}, \\ &\frac{D}{2}a(\vec{\phi},\vec{\phi}) + G\kappa t^{-2}b(\vec{\phi}, w; \vec{\phi}, w) \ge C_2 \|(\vec{\phi}, w)\|_{1,1,\Omega}^2, \end{aligned}$$

for all pairs $(\vec{\phi}, w)$, $(\vec{\theta}, \zeta) \in [H_0^1(\Omega)]^2 \times H_0^1(\Omega)$. Hence, by the Lax-Milgram lemma, (5) has a unique solution in $[H_0^1(\Omega)]^2 \times H_0^1(\Omega)$. Moreover, continuity and coercivity guarantee a unique solution to the discrete problem that follows.

The standard finite element discretization of (5) consists of constructing a pair of finite-dimensional subspaces $\vec{V}_N(\Omega) \subset [H_0^1(\Omega)]^2$, $W_N(\Omega) \subset H_0^1(\Omega)$ of

combined dimension N (the total number of degrees of freedom), and solving the problem: find $(\vec{\phi}_N, w_N) \in \vec{V}_N(\Omega) \times W_N(\Omega)$ such that

$$\frac{D}{2} a(\vec{\phi}_N, \vec{\theta}) + G\kappa t^{-2} b(\vec{\phi}_N, w_N; \vec{\theta}, \zeta) = \int_\Omega g\zeta \; dA \tag{8}$$

for all $(\vec{\theta}, \zeta) \in \vec{V}_N(\Omega) \times W_N(\Omega)$. The global spaces $\vec{V}_N(\Omega)$ for the rotation and $W_N(\Omega)$ for the midplane displacement are constructed by first partitioning the domain Ω into a mesh $\mathcal{M}$ of curvilinear quadrilateral and/or triangular elements Ω_k, each of which is the image of a reference element $\widehat{\Omega}$ under an invertible element mapping $\mathcal{F}_k : \widehat{\Omega} \to \Omega_k$. The reference element $\widehat{\Omega}$ is chosen as either the unit square $\widehat{S} = [-1, 1]^2$ or the reference triangle $\widehat{T} = \{(\xi, \eta) \in [0, 1]^2 : \eta \leq 1 - \xi\}$ (see figure 1). Then the global spaces $\vec{V}_N(\Omega),\ W_N(\Omega)$ are defined piecewise in the following way:

(1) Polynomial spaces $\widehat{V}_{p_1}(\widehat{\Omega})$ and $\widehat{W}_{p_2}(\widehat{\Omega})$ are chosen on the reference elements $\widehat{\Omega} = \widehat{S}$ or $\widehat{T}$, among

$$\mathcal{Q}_{p,q}(\widehat{\Omega}) = \text{span}\{\xi^i \eta^j : 0 \leq i \leq p, 0 \leq j \leq q\}, \tag{9}$$
$$\mathcal{Q}_p(\widehat{\Omega}) = \mathcal{Q}_{p,p}(\widehat{\Omega}), \tag{10}$$
$$\mathcal{P}_p(\widehat{\Omega}) = \text{span}\{\xi^i \eta^j : 0 \leq i + j \leq p\}. \tag{11}$$

(2) The reference spaces are mapped onto each element to create the spaces

$$\vec{V}_{p_1}(\Omega_k) = \left\{ \vec{\phi}_p = \widehat{\phi} \circ \mathcal{F}_k^{-1} : \widehat{\phi} \in \widehat{V}_{p_1}(\widehat{\Omega}) \right\}, \tag{12}$$
$$W_{p_2}(\Omega_k) = \left\{ w_q = \widehat{w} \circ \mathcal{F}_k^{-1} : \widehat{w} \in \widehat{W}_{p_2}(\widehat{\Omega}) \right\}. \tag{13}$$

(3) The global spaces are then defined by

$$\vec{V}_N(\Omega) = \left\{ \vec{\phi}_N \in H_0^1(\Omega) : \vec{\phi}_N|_{\Omega_k} \in \vec{V}_{p_1}(\Omega_k) \; \forall \Omega_k \in \mathcal{M} \right\}, \tag{14}$$
$$W_N(\Omega) = \left\{ w_N \in H_0^1(\Omega) : w_N|_{\Omega_k} \in W_{p_2}(\Omega_k) \; \forall \Omega_k \in \mathcal{M} \right\}. \tag{15}$$

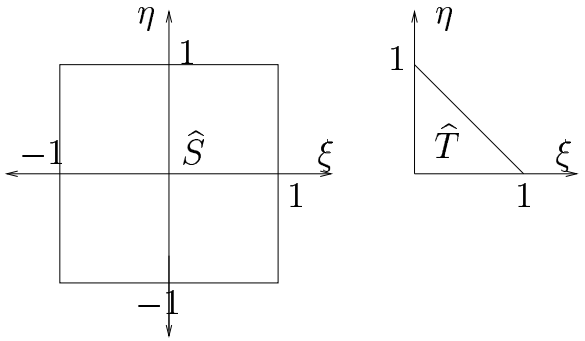

Fig. 1. Reference elements $\widehat{S}$ and $\widehat{T}$

The standard discretization (8) is highly sensitive to the plate thickness t. It is well known that the standard h version exhibits complete locking, unless polynomials of degree greater than 3 are used for the approximation. Unlike the h version, the high-order p and hp versions are free of locking as $p \to \infty$, when the error in the energy norm is of interest (see [16] for more details). Though it has been shown that standard p and hp version methods are free of locking, rigorous analyses have only been completed for meshes consisting of rectangular and straight sided triangular elements [14]. The analysis of the p/hp version for curvilinear meshes remains open, even though numerical evidence suggests that these methods are indeed asymptotically locking-free, even when certain curvilinear elements are used ([21], [25], [26]). However, standard methods do not yield satisfactory results when the moment and/or stress resultants are of interest (see e.g., [27]). In [19] this problem was somewhat alleviated through the use of the p version FEM along with a post-processing scheme for computing the resultants, and in particular the shear, equivalent to using the equilibrium (as opposed to the constitutive) relation. One of the main advantages of MITC methods, and the motivation behind our study, is that the need for such post-processing is eliminated since these methods approximate both the solution and the resultants well, without any additional computational effort. In addition, MITC methods have also been proven to work extremely well for the more difficult shell problem, for which curved elements are most useful (cf. [23]).

3 A p version MITC method

So-called MITC methods reduce the adverse effect of Kirchhoff's constraint on the approximation of thin plate problems. Since their introduction in 1989 by Brezzi, Bathe and Fortin [6], they have arguably become the "method of choice" for the approximation of plate problems. In this section we present the continuous and discrete MITC formulations, as well as give details for the implementation of an hp MITC method based on the Raviart-Thomas spaces [1].

3.1 Continuous Mixed Formulation

In this section, we outline a decomposition of (5) useful in the analysis of MITC methods. Our development closely follows that found in [18]. First, the scaled shear force

$$\vec{q} = G\kappa t^{-2}(\vec{\nabla} w - \vec{\phi}) \in [L^2(\Omega)]^2, \tag{16}$$

is introduced as an independent unknown in (5) to obtain the mixed formulation: find $\vec{\phi} \in [H_0^1(\Omega)]^2,\ w \in H_0^1(\Omega)$, and $\vec{q} \in [L^2(\Omega)]^2$ such that

$$\frac{D}{2}a(\vec{\phi},\vec{\theta}) + (\vec{q}, \vec{\nabla}\zeta - \vec{\theta}) = (g,\zeta), \tag{17}$$

$$(\vec{q},\vec{r}) - G\kappa t^{-2}(\vec{\nabla}w - \vec{\phi},\vec{r}) = 0 \tag{18}$$

for all $\vec{\theta} \in [H_0^1(\Omega)]^2,\ \zeta \in H_0^1(\Omega)$, and $\vec{r} \in [L^2(\Omega)]^2$. Equation (17) is simply a restatement of (5) with $G\kappa t^{-2}(\vec{\nabla}w - \vec{\phi})$ replaced by the new variable $\vec{q}$, and (18) guarantees that this replacement is valid.

For the next step, we will need the following version of the Helmholtz decomposition theorem [9]: Every $\vec{q} \in [L^2(\Omega)]^2$ has the unique decomposition

$$\vec{q} = \vec{\nabla}\psi + \vec{\mathrm{rot}}\ \rho, \tag{19}$$

where $\psi \in H_0^1(\Omega)$, $\rho \in H^1(\Omega) \cap L_0^2(\Omega)$, and

$$\vec{\mathrm{rot}}\ \rho = (\vec{\nabla}\rho)^{\perp} = \left\langle \frac{\partial\rho}{\partial y}, -\frac{\partial\rho}{\partial x} \right\rangle.$$

This decomposition allows us to split the mixed formulation (17)–(18) by making the substitutions [1]

$$\vec{q} = \vec{\nabla}\psi + \vec{\mathrm{rot}}\ \rho, \quad \vec{r} = \vec{\nabla}\xi + \vec{\mathrm{rot}}\ q,$$

which lead to the system: find $\vec{\phi} \in [H_0^1(\Omega)]^2,\ w \in H_0^1(\Omega),\ \psi \in H_0^1(\Omega)$, and $\rho \in H^1(\Omega) \cap L_0^2(\Omega)$ such that,

$$(\vec{\nabla}\psi, \vec{\nabla}\zeta) = (g,\zeta), \tag{20}$$

$$\frac{D}{2}a(\vec{\phi},\vec{\theta}) - (\vec{\nabla}\psi + \vec{\mathrm{rot}}\ \rho, \vec{\theta}) = 0, \tag{21}$$

$$(\vec{\mathrm{rot}}\ \rho, \vec{\mathrm{rot}}\ q) + G\kappa t^{-2}(\vec{\phi}, \vec{\mathrm{rot}}\ q) = 0, \tag{22}$$

$$(\vec{\nabla}\psi, \vec{\nabla}\xi) - G\kappa t^{-2}(\vec{\nabla}w - \vec{\phi}, \vec{\nabla}\xi) = 0 \tag{23}$$

for all $\vec{\theta} \in [H_0^1(\Omega)]^2,\ \zeta \in H_0^1(\Omega),\ \xi \in H_0^1(\Omega)$, and $q \in H^1(\Omega) \cap L_0^2(\Omega)$.

Finally, we will introduce

$$\vec{\alpha} = \vec{\mathrm{rot}}\ \rho \in H_0(\mathrm{rot}\ ;\Omega)$$

[1] Be sure to distinguish the scalar q from the scaled shear force $\vec{q}$.

as an independent unknown in (21)–(22), where the space $H_0(\text{rot };\Omega)$ is given by

$$H_0(\text{rot };\Omega) = \left\{ \vec{\alpha} \in [L^2(\Omega)]^2 : \text{rot } \vec{\alpha} \in L^2(\Omega),\ \vec{\alpha}\cdot\hat{t} = 0 \text{ on } \partial\Omega \right\}, \tag{24}$$

with $\hat{t}$ tangent to $\partial\Omega$ and the scalar rotation operator defined by

$$\text{rot } \vec{\alpha} = \vec{\nabla}\cdot\vec{\alpha}^{\perp} = \frac{\partial\alpha_2}{\partial x} - \frac{\partial\alpha_1}{\partial y}.$$

This substitution results in the system: find $\vec{\phi} \in [H_0^1(\Omega)]^2,\ w \in H_0^1(\Omega),\ \psi \in H_0^1(\Omega),\ \rho \in L_0^2(\Omega)$, and $\vec{\alpha} \in H_0(\text{rot };\Omega)$ such that

$$(\vec{\nabla}\psi, \vec{\nabla}\zeta) = (g,\zeta), \tag{25}$$

$$\frac{D}{2}a(\vec{\phi},\vec{\theta}) - (\rho, \text{rot } \vec{\theta}) - (\vec{\nabla}\psi,\vec{\theta}) = 0, \tag{26}$$

$$(\text{rot } \vec{\alpha}, q) + G\kappa t^{-2}(\text{rot } \vec{\phi}, q) = 0, \tag{27}$$

$$(\vec{\alpha},\vec{\delta}) - (\rho, \text{rot } \vec{\delta}) = 0, \tag{28}$$

$$(\vec{\nabla}\psi,\vec{\nabla}\xi) - G\kappa t^{-2}(\vec{\nabla}w - \vec{\phi},\vec{\nabla}\xi) = 0 \tag{29}$$

for all $\vec{\theta} \in [H_0^1(\Omega)]^2,\ \zeta \in H_0^1(\Omega),\ \xi \in H_0^1(\Omega),\ q \in L_0^2(\Omega)$, and $\vec{\delta} \in H_0(\text{rot };\Omega)$.

The final mixed formulation (25)–(29) is equivalent to the original one (17)–(18), but has the advantage that it can be treated as three independent problems. Namely, (25) can be solved first to obtain ψ, then (26)–(28) will yield $\vec{\phi}$, ρ, and $\vec{\alpha}$, and finally (29) can be solved for w. If an analogous decomposition can be obtained on the discrete level then error analyses can be carried out on these three problems separately.

3.2 Discretization

To define the MITC spaces we start with a known *stable*[2] space $\vec{V}_N$ for the rotation, and then project it, using a reduction operator $\mathbf{\Pi}_N$, onto a space of polynomials (see [18] for several choices of such spaces and reduction operators). These global spaces are defined using the usual reference spaces; however, as was shown in [24], curved elements require some "special" treatment. In particular, the basis for the reference space for the rotations is "split" into two disjoint subsets corresponding to the *internal* and *external* basis functions. The external basis functions are those which are non-zero along (at least

[2] The term stable means that the spaces satisfy the *inf-sup* condition.

one portion of) the boundary, while the internal basis functions are zero along the boundary and non-zero in the interior (see e.g., Ch. 6 in [11]). The space spanned by the external basis functions is mapped using the usual mapping in order to ensure inter-element continuity. The space spanned by the internal basis functions is mapped using a kind of *Piola* transform (see below and [24]).

The specific choices for the spaces used here correspond to Method 4 of [18] and Method 3 of [24]. Consequently, the rotation space $\vec{V}_N$ is defined for a mesh $\mathcal{M}$ composed of curvilinear quadrilaterals as follows.

(1) The reference space $\widehat{V}_p(\widehat{S})$ on the reference square is taken to be

$$\widehat{V}_p(\widehat{S}) = [\mathcal{Q}_{p+1}(\widehat{S})]^2 = \widehat{V}_p^0(\widehat{S}) \oplus \widehat{V}_p^e(\widehat{S}).$$

The superscript 0 is used to denote the subspace of functions zero on $\partial\widehat{S}$ (i.e., the space spanned by the internal basis functions), and e denotes functions nonzero on $\partial\widehat{S}$ (i.e., the space spanned by the external basis functions).

(2) The element space $\vec{V}_p(S_k)$ is defined by

$$\begin{aligned}\vec{V}_p(S_k) &= \vec{V}_p^0(S_k) \oplus \vec{V}_p^e(S_k) \\ &= \left\{\vec{\phi} = J_k^{-T}\widehat{\phi} \circ \mathcal{F}_k^{-1} \ : \ \widehat{\phi} \in \widehat{V}_p^0(\widehat{S})\right\} \\ &\quad \oplus \left\{\vec{\phi} = \widehat{\phi} \circ \mathcal{F}_k^{-1} \ : \ \widehat{\phi} \in \widehat{V}_p^e(\widehat{S})\right\} \end{aligned} \tag{30}$$

where $S_k = \mathcal{F}_k(\widehat{S})$ and J_k^{-T} is the inverse transpose of the derivative of the element mapping $\mathcal{F}_k$. Notice the modified mapping used for the internal shape functions.

(3) The global space $\vec{V}_N$ is defined by

$$\vec{V}_N = \left\{\vec{\phi} \in [H_0^1(\Omega)]^2 : \vec{\phi}|_{S_k} \in \vec{V}_p(S_k), \ \forall S_k \in \mathcal{M}\right\}.$$

The midplane displacement space $W_N(\Omega)$ is obtained in the usual manner using (13) and (15) with $\widehat{W}_p(\widehat{\Omega}) = Q_p(\widehat{\Omega})$.

The space $\vec{V}_N$ is projected by a reduction operator $\mathbf{\Pi}_N$, defined elementwise by

$$(\mathbf{\Pi}_N\vec{\phi})|_{S_k} = \begin{cases} J^{-T}(\widehat{\mathbf{\Pi}}_p\widehat{\phi}) \circ \mathcal{F}_k^{-1} & \text{for } \vec{\phi}|_{S_k} \in \vec{V}_p^0(S_k) \\ (\widehat{\mathbf{\Pi}}_p\widehat{\phi}) \circ \mathcal{F}_k^{-1} & \text{for } \vec{\phi}|_{S_k} \in \vec{V}_p^e(S_k) \end{cases},$$

where the reference projection $\widehat{\mathbf{\Pi}}_p$ is a strategically chosen projection onto a space of polynomials. In our study, we choose the Raviart-Thomas spaces

$\mathcal{Q}_{p-1,p}(\widehat{S}) \times \mathcal{Q}_{p,p-1}(\widehat{S})$ (see [1] and [9]), even though other choices are possible, e.g. the BDFM spaces [3]. Specifically, the conditions defining $\widehat{\mathbf{\Pi}}_p$ are

$$\int_{\widehat{E}} ((\widehat{\mathbf{\Pi}}_p \hat{\phi} - \hat{\phi}) \cdot \vec{t}) \hat{v} = 0, \quad \text{for all } \hat{v} \in \mathcal{P}_{p-1}(\widehat{E}) \text{ for every edge } \widehat{E} \text{ of } \widehat{S}, \tag{31}$$

$$\int_{\widehat{S}} (\widehat{\mathbf{\Pi}}_p \hat{\phi} - \hat{\phi}) \cdot \hat{r} = 0, \quad \text{for all } \hat{r} \in \mathcal{Q}_{p-1,p-2}(\widehat{S}) \times \mathcal{Q}_{p-2,p-1}(\widehat{S}). \tag{32}$$

The resulting discrete problem is: find $(\vec{\phi}_N, w_N) \in \vec{V}_N(\Omega) \times W_N(\Omega)$ such that for all $(\vec{\theta}, \zeta) \in \vec{V}_N(\Omega) \times W_N(\Omega)$

$$\frac{D}{2} a(\vec{\phi}_N, \vec{\theta}) + G\kappa t^{-2} b(\mathbf{\Pi}_N \vec{\phi}_N, w_N; \mathbf{\Pi}_N \vec{\theta}, \zeta) = \int_\Omega g\zeta \; dA. \tag{33}$$

3.3 Implementation

We have implemented the method described by (33) and include here expanded forms for some of the deceptively simple expressions in (33) needed in the implementation. To solve (33), all of the functions and integrals involved are restricted to a single element S_k, the resulting element matrix and load vector are constructed, and then assembled into a global system.

To facilitate the computation of the element matrix for element S_k from (33), we will begin by rewriting the bilinear form in (6) as

$$\begin{aligned} a(\vec{\phi}, \vec{\theta}) = 2 \int_{S_k} \Bigg[& \frac{\partial \phi_1}{\partial x}\frac{\partial \theta_1}{\partial x} + \nu \left(\frac{\partial \phi_1}{\partial x}\frac{\partial \theta_2}{\partial y} + \frac{\partial \phi_2}{\partial y}\frac{\partial \theta_1}{\partial x} \right) + \frac{\partial \phi_2}{\partial y}\frac{\partial \theta_2}{\partial y} \\ & + \bar{\nu} \left(\frac{\partial \phi_1}{\partial y} + \frac{\partial \phi_2}{\partial x} \right) \left(\frac{\partial \theta_1}{\partial y} + \frac{\partial \theta_2}{\partial x} \right) \Bigg] dxdy \end{aligned} \tag{34}$$

where $\bar{\nu} = (1 - \nu)/2$. Notice that this restatement leaves b unchanged

$$\begin{aligned} b(\vec{\phi}, w; \vec{\theta}, \zeta) = \int_{S_k} \Bigg[& \left(\frac{\partial w}{\partial x} - \phi_1 \right) \left(\frac{\partial \zeta}{\partial x} - \theta_1 \right) + \\ & + \left(\frac{\partial w}{\partial y} - \phi_2 \right) \left(\frac{\partial \zeta}{\partial y} - \theta_2 \right) \Bigg] dxdy. \end{aligned} \tag{35}$$

On each element, the solution is expanded as a linear combination of mapped basis functions $\widehat{N}_i(\xi, \eta)$, as follows:

$$
\begin{aligned}
\vec{\phi}(x,y) &= \vec{\phi}^0(x,y) + \vec{\phi}^e(x,y) \\
&= \sum_i J_k^{-T} \begin{pmatrix} \phi_1^i \\ \phi_2^i \end{pmatrix} \widehat{N}_i(\xi,\eta) + \sum_j \begin{pmatrix} \phi_1^j \\ \phi_2^j \end{pmatrix} \widehat{N}_j(\xi,\eta) \\
&= \sum_i \begin{pmatrix} \dfrac{\partial \xi}{\partial x}\phi_1^i + \dfrac{\partial \eta}{\partial x}\phi_2^i \\ \dfrac{\partial \xi}{\partial y}\phi_1^i + \dfrac{\partial \eta}{\partial y}\phi_2^i \end{pmatrix} \widehat{N}_i(\xi,\eta) + \sum_j \begin{pmatrix} \phi_1^j \\ \phi_2^j \end{pmatrix} \widehat{N}_j(\xi,\eta)
\end{aligned}
$$

where i indexes the internal, and j the external basis functions. Since we are interested in the p version, we utilize the hierarchical basis functions constructed from integrated Legendre polynomials (see Ch. 6 in [11] for details). In addition, this set of basis functions is naturally divided into external and internal functions, hence the non-traditional mapping of the internal basis functions does not further complicate the implementation of the method.

In order to plug the above expansion into (34) we will need expressions for the derivatives

$$
\frac{\partial \phi_1}{\partial x} = \sum_j \phi_1^j \xi_{xx}^j + \phi_2^j \eta_{xx}^j, \quad \frac{\partial \phi_1}{\partial y} = \sum_j \phi_1^j \xi_{xy}^j + \phi_2^j \eta_{xy}^j, \tag{36}
$$

$$
\frac{\partial \phi_2}{\partial x} = \sum_j \phi_1^j \xi_{yx}^j + \phi_2^j \eta_{yx}^j, \quad \frac{\partial \phi_2}{\partial y} = \sum_j \phi_1^j \xi_{yy}^j + \phi_2^j \eta_{yy}^j, \tag{37}
$$

where j now indexes all basis functions, and

$$
\xi_{xx}^j = \begin{cases} \dfrac{\partial^2 \xi}{\partial x^2}\widehat{N}_j + \dfrac{\partial \xi}{\partial x}\dfrac{\partial \widehat{N}_j}{\partial x} \\ \dfrac{\partial \widehat{N}_j}{\partial x} \end{cases} \qquad \eta_{xx}^j = \begin{cases} \dfrac{\partial^2 \eta}{\partial x^2}\widehat{N}_j + \dfrac{\partial \eta}{\partial x}\dfrac{\partial \widehat{N}_j}{\partial x} \\ 0 \cdot \end{cases}
$$

$$
\xi_{xy}^j = \begin{cases} \dfrac{\partial^2 \xi}{\partial y \partial x}\widehat{N}_j + \dfrac{\partial \xi}{\partial x}\dfrac{\partial \widehat{N}_j}{\partial y} \\ \dfrac{\partial \widehat{N}_j}{\partial y} \end{cases} \qquad \eta_{xy}^j = \begin{cases} \dfrac{\partial^2 \eta}{\partial y \partial x}\widehat{N}_j + \dfrac{\partial \eta}{\partial x}\dfrac{\partial \widehat{N}_j}{\partial y} \\ 0 \cdot \end{cases}
$$

$$
\xi_{yx}^j = \begin{cases} \dfrac{\partial^2 \xi}{\partial x \partial y}\widehat{N}_j + \dfrac{\partial \xi}{\partial y}\dfrac{\partial \widehat{N}_j}{\partial x} \\ 0 \cdot \end{cases} \qquad \eta_{yx}^j = \begin{cases} \dfrac{\partial^2 \eta}{\partial x \partial y}\widehat{N}_j + \dfrac{\partial \eta}{\partial y}\dfrac{\partial \widehat{N}_j}{\partial x} \\ \dfrac{\partial \widehat{N}_j}{\partial x} \end{cases}
$$

$$\xi^j_{yy} = \begin{cases} \dfrac{\partial^2 \xi}{\partial y^2}\widehat{N}_j + \dfrac{\partial \xi}{\partial y}\dfrac{\partial \widehat{N}_j}{\partial y} \\ \\ 0. \end{cases} \qquad \eta^j_{yy} = \begin{cases} \dfrac{\partial^2 \eta}{\partial y^2}\widehat{N}_j + \dfrac{\partial \eta}{\partial y}\dfrac{\partial \widehat{N}_j}{\partial y} \\ \\ \dfrac{\partial \widehat{N}_j}{\partial y} \end{cases}$$

(the top expressions are valid if j is the index of an internal basis function; the bottom expressions are valid otherwise). We will need to express these quantities as functions of the reference coordinates (ξ, η) in order to make a change of variables in the integral (34). The first derivatives are obtained easily using the inverse function theorem

$$J_k^{-1}(x, y) = \left[J_k(\xi, \eta)\right]^{-1},$$

and explicitly inverting J_k

$$\begin{bmatrix} \dfrac{\partial \xi}{\partial x} & \dfrac{\partial \xi}{\partial y} \\ \dfrac{\partial \eta}{\partial x} & \dfrac{\partial \eta}{\partial y} \end{bmatrix} = \begin{bmatrix} \dfrac{\partial x}{\partial \xi} & \dfrac{\partial x}{\partial \eta} \\ \dfrac{\partial y}{\partial \xi} & \dfrac{\partial y}{\partial \eta} \end{bmatrix}^{-1} = \frac{1}{|J_k|} \begin{bmatrix} \dfrac{\partial y}{\partial \eta} & -\dfrac{\partial x}{\partial \eta} \\ -\dfrac{\partial y}{\partial \xi} & \dfrac{\partial x}{\partial \xi} \end{bmatrix}.$$

Thus,

$$\begin{aligned} \frac{\partial \xi}{\partial x} &= \frac{1}{|J_k|}\frac{\partial y}{\partial \eta}, \ \frac{\partial \xi}{\partial y} = -\frac{1}{|J_k|}\frac{\partial x}{\partial \eta}, \\ \frac{\partial \eta}{\partial x} &= -\frac{1}{|J_k|}\frac{\partial y}{\partial \xi}, \ \frac{\partial \eta}{\partial y} = \frac{1}{|J_k|}\frac{\partial x}{\partial \xi}. \end{aligned}$$

From these expressions the second derivatives become

$$\begin{aligned} \frac{\partial^2 \xi}{\partial x^2} &= +\frac{1}{|J_k|}\left[\frac{\partial^2 y}{\partial \xi \partial \eta}\frac{\partial \xi}{\partial x} + \frac{\partial^2 y}{\partial \eta^2}\frac{\partial \eta}{\partial x}\right] - \frac{1}{|J_k|}\frac{\partial |J_k|}{\partial x}\frac{\partial \xi}{\partial x}, \\ \frac{\partial^2 \xi}{\partial y \partial x} &= +\frac{1}{|J_k|}\left[\frac{\partial^2 y}{\partial \xi \partial \eta}\frac{\partial \xi}{\partial y} + \frac{\partial^2 y}{\partial \eta^2}\frac{\partial \eta}{\partial y}\right] - \frac{1}{|J_k|}\frac{\partial |J_k|}{\partial y}\frac{\partial \xi}{\partial x}, \\ \frac{\partial^2 \xi}{\partial x \partial y} &= -\frac{1}{|J_k|}\left[\frac{\partial^2 x}{\partial \xi \partial \eta}\frac{\partial \xi}{\partial x} + \frac{\partial^2 x}{\partial \eta^2}\frac{\partial \eta}{\partial x}\right] - \frac{1}{|J_k|}\frac{\partial |J_k|}{\partial x}\frac{\partial \xi}{\partial y}, \\ \frac{\partial^2 \xi}{\partial y^2} &= -\frac{1}{|J_k|}\left[\frac{\partial^2 x}{\partial \xi \partial \eta}\frac{\partial \xi}{\partial y} + \frac{\partial^2 x}{\partial \eta^2}\frac{\partial \eta}{\partial y}\right] - \frac{1}{|J_k|}\frac{\partial |J_k|}{\partial y}\frac{\partial \xi}{\partial y}, \\ \frac{\partial^2 \eta}{\partial x^2} &= -\frac{1}{|J_k|}\left[\frac{\partial^2 y}{\partial \xi^2}\frac{\partial \xi}{\partial x} + \frac{\partial^2 y}{\partial \xi \partial \eta}\frac{\partial \eta}{\partial x}\right] - \frac{1}{|J_k|}\frac{\partial |J_k|}{\partial x}\frac{\partial \eta}{\partial x}, \\ \frac{\partial^2 \eta}{\partial y \partial x} &= -\frac{1}{|J_k|}\left[\frac{\partial^2 y}{\partial \xi^2}\frac{\partial \xi}{\partial y} + \frac{\partial^2 y}{\partial \xi \partial \eta}\frac{\partial \eta}{\partial y}\right] - \frac{1}{|J_k|}\frac{\partial |J_k|}{\partial y}\frac{\partial \eta}{\partial x}, \end{aligned}$$

$$\frac{\partial^2\eta}{\partial x\partial y} = +\frac{1}{|J_k|}\left[\frac{\partial^2 x}{\partial\xi^2}\frac{\partial\xi}{\partial x} + \frac{\partial^2 x}{\partial\xi\partial\eta}\frac{\partial\eta}{\partial x}\right] - \frac{1}{|J_k|}\frac{\partial|J_k|}{\partial x}\frac{\partial\eta}{\partial y},$$
$$\frac{\partial^2\eta}{\partial y^2} = +\frac{1}{|J_k|}\left[\frac{\partial^2 x}{\partial\xi^2}\frac{\partial\xi}{\partial y} + \frac{\partial^2 x}{\partial\xi\partial\eta}\frac{\partial\eta}{\partial y}\right] - \frac{1}{|J_k|}\frac{\partial|J_k|}{\partial y}\frac{\partial\eta}{\partial y}.$$

Now, we separate the integrand from (34) into three parts

$$\int_{S_k}\left(\frac{\partial\phi_1}{\partial x}\frac{\partial\theta_1}{\partial x} + \frac{\partial\phi_2}{\partial y}\frac{\partial\theta_2}{\partial y}\right)dxdy = \begin{bmatrix}\vec{\theta}_1 & \vec{\theta}_2\end{bmatrix}\begin{bmatrix}G_{00} & G_{01}\\ G_{10} & G_{11}\end{bmatrix}\begin{bmatrix}\vec{\phi}_1\\ \vec{\phi}_2\end{bmatrix} \tag{38}$$

$$\int_{S_k}\left(\frac{\partial\phi_1}{\partial x}\frac{\partial\theta_2}{\partial y} + \frac{\partial\phi_2}{\partial y}\frac{\partial\theta_1}{\partial x}\right)dxdy = \begin{bmatrix}\vec{\theta}_1 & \vec{\theta}_2\end{bmatrix}\begin{bmatrix}D_{00} & D_{01}\\ D_{10} & D_{11}\end{bmatrix}\begin{bmatrix}\vec{\phi}_1\\ \vec{\phi}_2\end{bmatrix} \tag{39}$$

$$\int_{S_k}\left(\frac{\partial\phi_1}{\partial y} + \frac{\partial\phi_2}{\partial x}\right)\left(\frac{\partial\theta_1}{\partial y} + \frac{\partial\theta_2}{\partial x}\right)dxdy = \begin{bmatrix}\vec{\theta}_1 & \vec{\theta}_2\end{bmatrix}\begin{bmatrix}R_{00} & R_{01}\\ R_{10} & R_{11}\end{bmatrix}\begin{bmatrix}\vec{\phi}_1\\ \vec{\phi}_2\end{bmatrix} \tag{40}$$

so that

$$a(\vec{\phi},\vec{\theta}) = 2\begin{bmatrix}\vec{\theta}_1 & \vec{\theta}_2\end{bmatrix}\begin{bmatrix}G_{00}+\nu D_{00}+\overline{\nu}R_{00} & G_{01}+\nu D_{01}+\overline{\nu}R_{01}\\ G_{10}+\nu D_{10}+\overline{\nu}R_{10} & G_{11}+\nu D_{11}+\overline{\nu}R_{11}\end{bmatrix}\begin{bmatrix}\vec{\phi}_1\\ \vec{\phi}_2\end{bmatrix}.$$

Here, $\vec{\phi}_1$ and $\vec{\phi}_2$ are coefficient vectors for ϕ_1 and ϕ_2. We will now show how to obtain expressions for the entries of the matrix G and state the analogous expressions for D and R. In the left hand side of (38) we use the expansions in (36)–(37) for $\vec{\phi}$ and analogous ones for $\vec{\theta}$ to obtain

$$\begin{aligned}\frac{\partial\phi_1}{\partial x}\frac{\partial\theta_1}{\partial x} + \frac{\partial\phi_2}{\partial y}\frac{\partial\theta_2}{\partial y} &= \left(\sum_j \phi_1^j\xi_{xx}^j + \phi_2^j\eta_{xx}^j\right)\left(\sum_i \theta_1^i\xi_{xx}^i + \theta_2^i\eta_{xx}^i\right)\\ &\quad + \left(\sum_j \phi_1^j\xi_{yy}^j + \phi_2^j\eta_{yy}^j\right)\left(\sum_i \theta_1^i\xi_{yy}^i + \theta_2^i\eta_{yy}^i\right)\\ &= \sum_{i,j}\theta_1^i(\xi_{xx}^i\xi_{xx}^j + \xi_{yy}^i\xi_{yy}^j)\phi_1^j + \theta_1^i(\xi_{xx}^i\eta_{xx}^j + \xi_{yy}^i\eta_{yy}^j)\phi_2^j\\ &\quad + \theta_2^i(\eta_{xx}^i\xi_{xx}^j + \eta_{yy}^i\xi_{yy}^j)\phi_1^j + \theta_2^i(\eta_{xx}^i\eta_{xx}^j + \eta_{yy}^i\eta_{yy}^j)\phi_2^j.\end{aligned}$$

Similarly, the right hand side of (38) can be expanded as

$$\begin{aligned}&\vec{\theta}_1 G_{00}\vec{\phi}_1 + \vec{\theta}_1 G_{01}\vec{\phi}_2 + \vec{\theta}_2 G_{10}\vec{\phi}_1 + \vec{\theta}_2 G_{11}\vec{\phi}_2\\ &= \sum_{i,j}\theta_1^i\left[G_{00}\right]_{ij}\phi_1^j + \theta_1^i\left[G_{01}\right]_{ij}\phi_2^j + \theta_2^i\left[G_{10}\right]_{ij}\phi_1^j + \theta_2^i\left[G_{11}\right]_{ij}\phi_2^j.\end{aligned}$$

By matching terms in the previous two sums and changing variables in the integrals in (38) we obtain

$$
\begin{aligned}
[G_{00}]_{ij} &= \int_{\widehat{S}} \left(\xi^i_{xx} \xi^j_{xx} + \xi^i_{yy} \xi^j_{yy} \right) |J_k| d\xi d\eta, \\
[G_{01}]_{ij} &= \int_{\widehat{S}} \left(\xi^i_{xx} \eta^j_{xx} + \xi^i_{yy} \eta^j_{yy} \right) |J_k| d\xi d\eta, \\
[G_{10}]_{ij} &= \int_{\widehat{S}} \left(\eta^i_{xx} \xi^j_{xx} + \eta^i_{yy} \xi^j_{yy} \right) |J_k| d\xi d\eta, \\
[G_{11}]_{ij} &= \int_{\widehat{S}} \left(\eta^i_{xx} \eta^j_{xx} + \eta^i_{yy} \eta^j_{yy} \right) |J_k| d\xi d\eta.
\end{aligned}
$$

By similar means

$$
\begin{aligned}
[D_{00}]_{ij} &= \int_{\widehat{S}} \left(\xi^i_{yy} \xi^j_{xx} + \xi^i_{xx} \xi^j_{yy} \right) |J_k| d\xi d\eta, \\
[D_{01}]_{ij} &= \int_{\widehat{S}} \left(\xi^i_{yy} \eta^j_{xx} + \xi^i_{xx} \eta^j_{yy} \right) |J_k| d\xi d\eta, \\
[D_{10}]_{ij} &= \int_{\widehat{S}} \left(\eta^i_{yy} \xi^j_{xx} + \eta^i_{xx} \xi^j_{yy} \right) |J_k| d\xi d\eta, \\
[D_{11}]_{ij} &= \int_{\widehat{S}} \left(\eta^i_{yy} \eta^j_{xx} + \eta^i_{xx} \eta^j_{yy} \right) |J_k| d\xi d\eta, \\
[R_{00}]_{ij} &= \int_{\widehat{S}} \left(\xi^i_{yx} + \xi^i_{xy} \right) \left(\xi^j_{yx} + \xi^j_{xy} \right) |J_k| d\xi d\eta, \\
[R_{01}]_{ij} &= \int_{\widehat{S}} \left(\xi^i_{yx} + \xi^i_{xy} \right) \left(\eta^j_{yx} + \eta^j_{xy} \right) |J_k| d\xi d\eta, \\
[R_{10}]_{ij} &= \int_{\widehat{S}} \left(\eta^i_{yx} + \eta^i_{xy} \right) \left(\xi^j_{yx} + \xi^j_{xy} \right) |J_k| d\xi d\eta, \\
[R_{11}]_{ij} &= \int_{\widehat{S}} \left(\eta^i_{yx} + \eta^i_{xy} \right) \left(\eta^j_{yx} + \eta^j_{xy} \right) |J_k| d\xi d\eta.
\end{aligned}
$$

The global linear system is constructed from the above elemental expressions in the usual manner (including possibly static condensation [11]). For additional implementational details see [26].

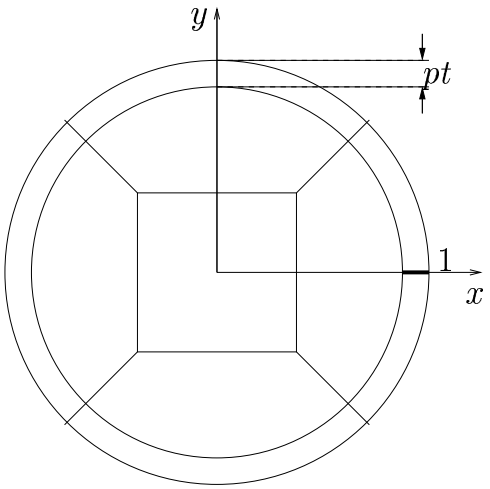

Fig. 2. 9-element unit-circular mesh with boundary refinement

4 Numerical experiments

In this section we present the results of numerical computations for two model problems with known exact solutions [5], in order to accurately assess the performance of the method. The results presented here are for a unit circular plate with Young's modulus $E = 1$, Poisson ratio $\nu = 0.3$, shear correction factor $\kappa = 1$, and transverse load density given in polar coordinates by

$$g(r, \theta) = \cos(\theta).$$

The mesh (shown in figure 2) was designed according to the recommendations of [21] and it includes thin elements of width pt along the boundary of the domain in order for the boundary layer to be uniformly approximated [3]. Here p is the degree of the approximating polynomial, which is increased from $p = 1$ to $p = 8$ for our computations, and t is the plate thickness which was chosen as $t = 10^{-j}, j = 2, 3, 4$. We note that no approximation to the boundary of the plate is made, but rather the curved elements are mapped exactly, using the blending map technique (cf. [11], pp. 107–108) to construct the element mappings F_k. For simplicity, we have only implemented the method for quadrilateral elements, even though the implementation can be modified for triangular elements in a straight-forward manner.

We will be plotting the error measured in the energy norm

$$\|(\vec{\phi}, w)\|_E^2 = \frac{D}{2} a(\vec{\phi}, \vec{\phi}) + G\kappa t^{-2} b(\vec{\phi}, w; \vec{\phi}, w) \tag{41}$$

[3] If the boundary layer is not well approximated then any computed results will not be accurate uniformly in t; this occurs when, e.g., a uniform mesh is used (cf. [21], [22]).

versus the number of degrees of freedom N, in a semi-log scale, as calculated using the p-MITC and the standard finite element method. In addition to (41), we are also interested in the pointwise error in the stress and moment resultants, and for concreteness we will concentrate on the approximation of the shear force. For the MITC formulation the shear force will be computed using

$$\vec{Q}_N = -G\kappa t^{-2}(\vec{\nabla} w_N - \mathbf{\Pi}_N \vec{\phi}_N) \tag{42}$$

while for the standard formulation the shear force will be computed using the constitutive relation (4), as well as the equilibrium equation, which basically amounts to a post-processing scheme – the computations for this last case will be performed using the commercial finite element code StressCheck (E.S.R.D., St. Louis, MO). We should point out that $\vec{Q}_N$ given by (42) is often referred to as *projected shear* (cf. [28]), and it gives a better approximation than the one obtained by equation (4) (with $w, \vec{\phi}$ replaced by $w_N, \vec{\phi}_N$) (see [18] for details). The fact that the projection operator $\mathbf{\Pi}_N$ is an integral part of the MITC formulation is the reason we do not refer to this as "post-processing".

Since $\vec{Q} \notin L^2(\Omega)$ as $t \to 0$, one cannot expect pointwise approximations to have any accuracy uniformly in t, especially near the boundary. For this reason we will compute $\vec{Q}$ sufficiently away from the boundary; in particular we will be measuring the first component of the shear force $Q_x(x, 0)$, for $0 \leq x \leq 1-pt$, with $p = 8$ (the highest approximating polynomial degree).

4.1 Clamped plate

First we consider a clamped plate, for which the boundary layer is weak [15]. Figures 3–5 show the error measured in the energy norm, as computed by both the standard and MITC formulations. As these figures indicate, both methods perform well, independently of the thickness t, and near exponential convergence rates are observed. (These rates can also be interpreted as arbitrarily high algebraic convergence.)

Figures 6–8 show the shear force distribution, as well as the error in the shear force, for the standard formulation (with and without post-processing) and for the MITC formulation. First, we note that for $t = 0.01$ (see figure 6) most of the error comes from the center of the plate, while as t gets smaller (see figures 7,8) the error closer to the boundary dominates – this is more so for the standard formulation(s) than for the MITC method. This is due to the fact that the mesh (see figure 2) is coarse and only one element is used in the middle of the plate. Even though adding more elements in the interior would

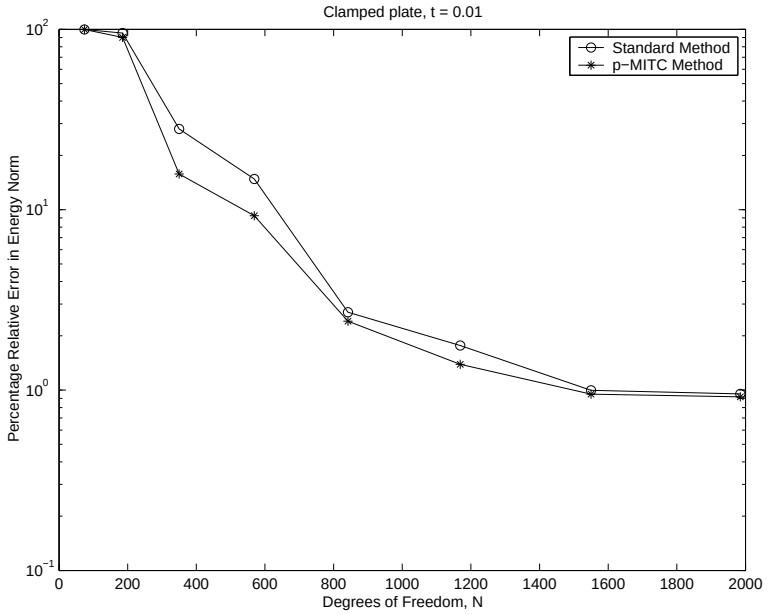

Fig. 3. Energy norm convergence for the clamped plate, $t = 0.01$.

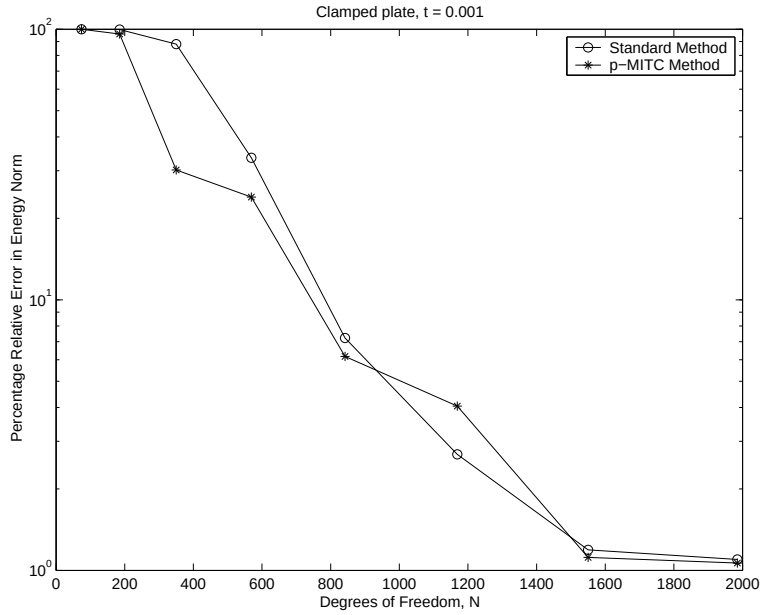

Fig. 4. Energy norm convergence for the clamped plate, $t = 0.001$.

improve the situation for all methods, we see that the MITC formulation performs quite well without additional refinement.

These figures also confirm that post-processing the FEM solution is *necessary* if one uses the standard formulation (especially as $t \to 0$). But most importantly, they show that the MITC formulation performs at least as well as the standard formulation with post-processing, and visibly better as $t \to 0$, without the need for additional post-processing (beyond the fact that (42) is

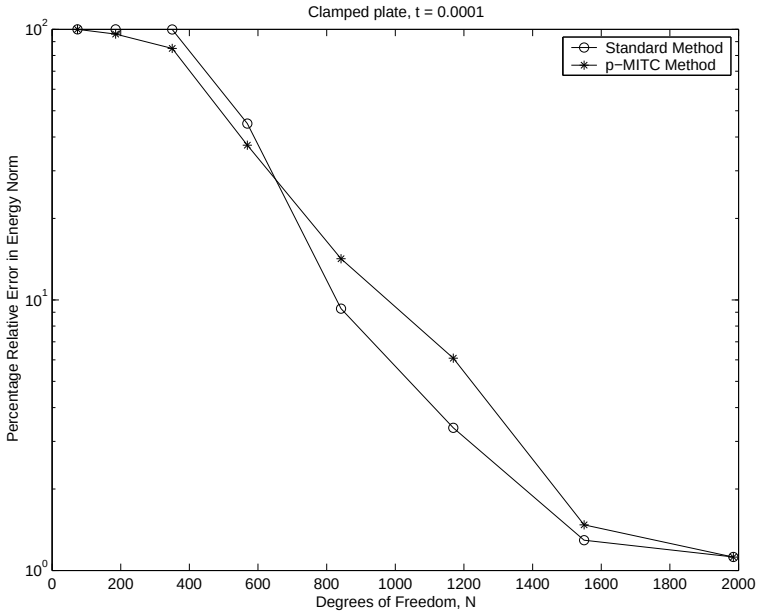

Fig. 5. Energy norm convergence for the clamped plate, $t = 0.0001$.

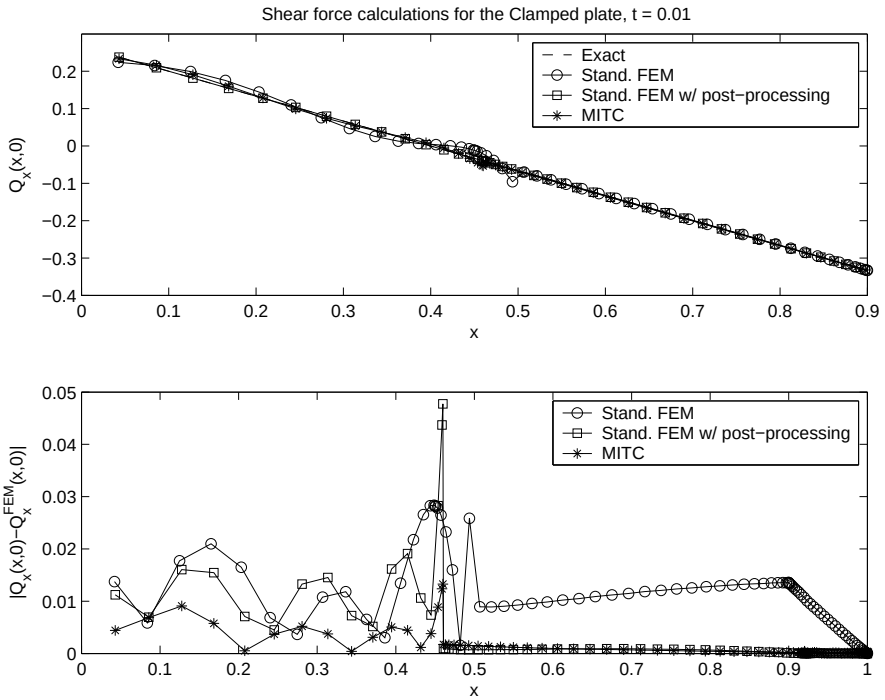

Fig. 6. Shear force computations for the clamped plate, $t = 0.01$.

used).

Finally, figure 9 shows the convergence of the computed shear at the center of the plate, for both the standard formulation with post-processing and the p-MITC formulation. In particular, we plot the percentage relative error in $Q_x(0,0)$, versus the polynomial degree p in a semilog scale, for $t = 0.01$. (For

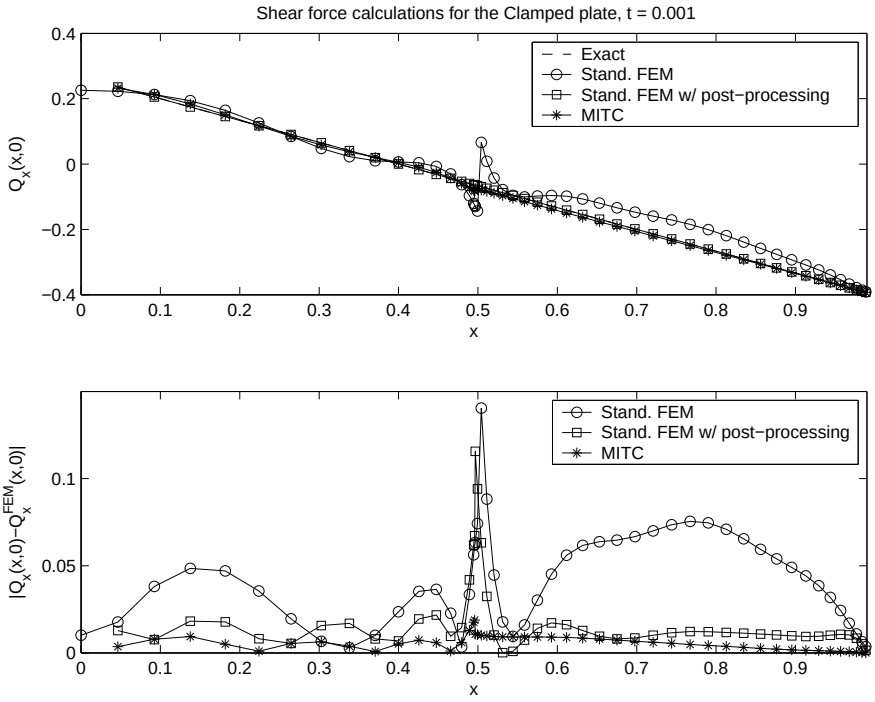

Fig. 7. Shear force computations for the clamped plate, $t = 0.001$.

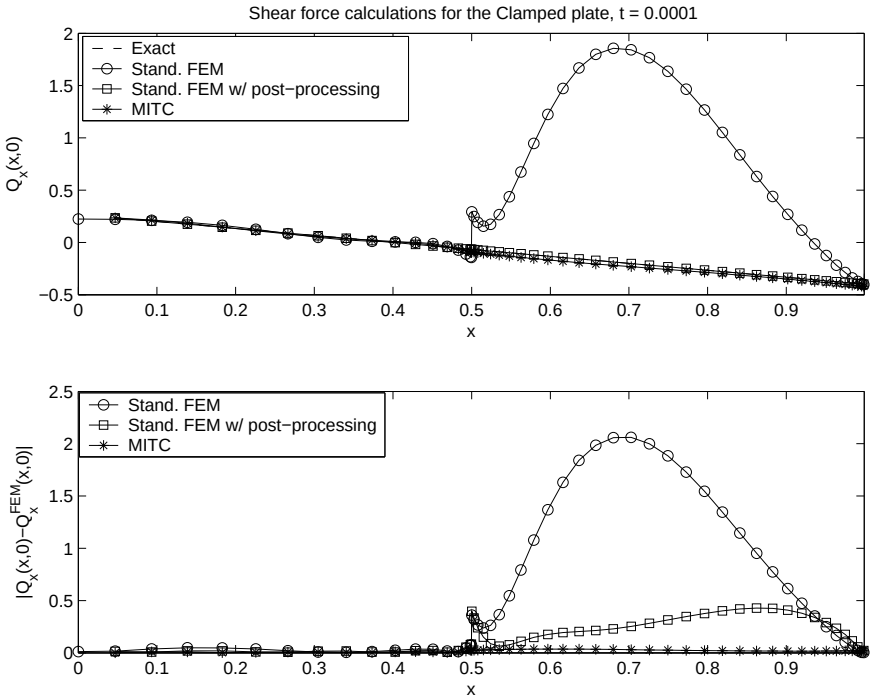

Fig. 8. Shear force computations for the clamped plate, $t = 0.0001$.

different thickness the plots are similar to the one shown here). We see that both methods converge at an observed near exponential rate, with the p-MITC method having a slight advantage. (See also [18], [28] for L^2 error estimates for

the shear in the case of quasiuniform, and locally quasiuniform meshes with straight sided elements.)

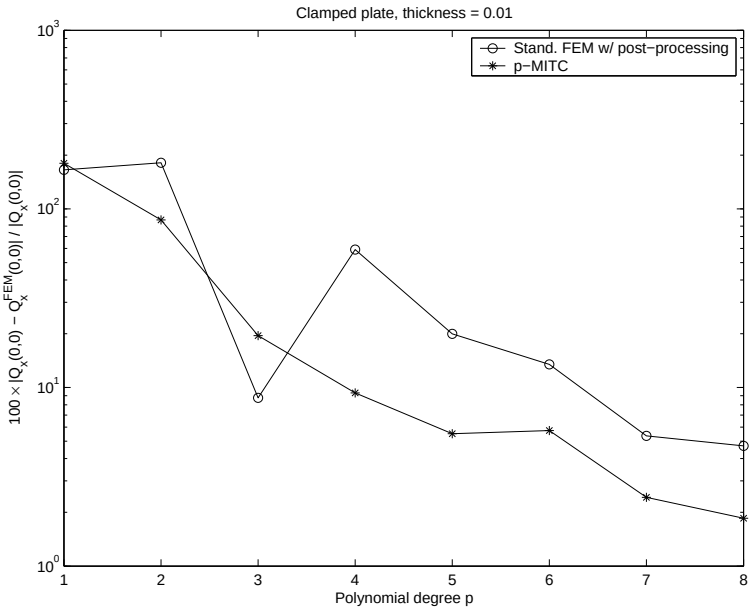

Fig. 9. Convergence of the shear force at (0,0) for the clamped plate, $t = 0.01$.

4.2 Soft-Simply-Supported plate

We now repeat the previous experiments for the case of a soft-simply-supported plate, keeping all material constants and loads the same as before. In this case the boundary layer is stronger [4], hence the proper mesh design is of utmost importance (cf. [21]). Figures 10–12 show the energy norm convergence for both methods and, as before, we observe that their performance is not affected by $t \to 0$ and all three seem to be converging near exponentially.

The shear force (and the associated errors) are shown in figures 13–15. With the exception of $t = 0.0001$, the results are almost identical to the previous example, and once again confirm that MITC methods are excellent for the approximation of plate problems, even in the presence of curved elements. For $t = 0.0001$ (see figure 15) we see that the standard formulation without post-processing yields extremely high errors, while the performance of the other two methods begins to deteriorate as we get closer to the boundary, due to the lack of smoothness of Q_x.

Finally, figure 16 shows the convergence for the standard and MITC formulations, as was done in the previous example, with identical conclusions.

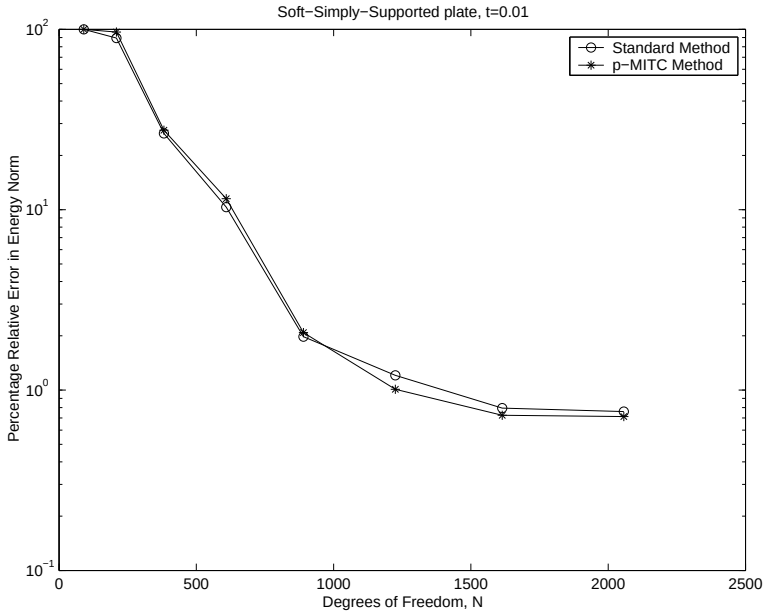

Fig. 10. Energy norm convergence for the S-S-S plate, $t = 0.01$.

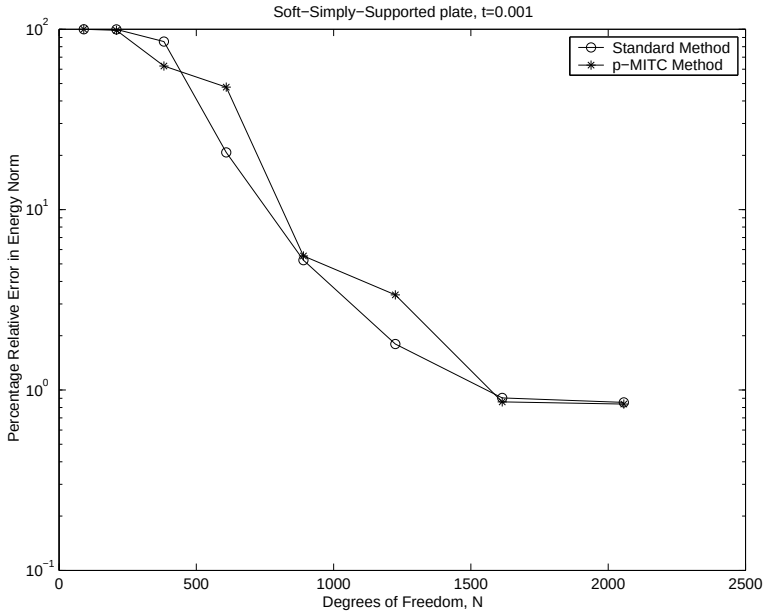

Fig. 11. Energy norm convergence for the S-S-S plate, $t = 0.001$.

5 Conclusions

We have studied the approximation of the Reissner-Mindlin plates with curved boundaries by a p version MITC finite element method. By combining the ideas of [18] on hp MITC methods and of [24] on curved elements, we were able to successfully formulate and implement the method. Our numerical computations confirmed that p–MITC elements are extremely effective for plate

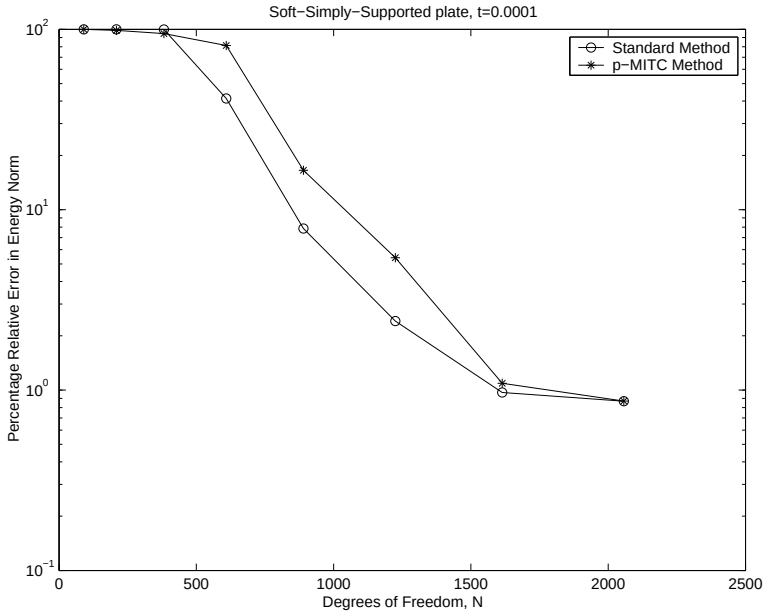

Fig. 12. Energy norm convergence for the S-S-S plate, $t = 0.0001$.

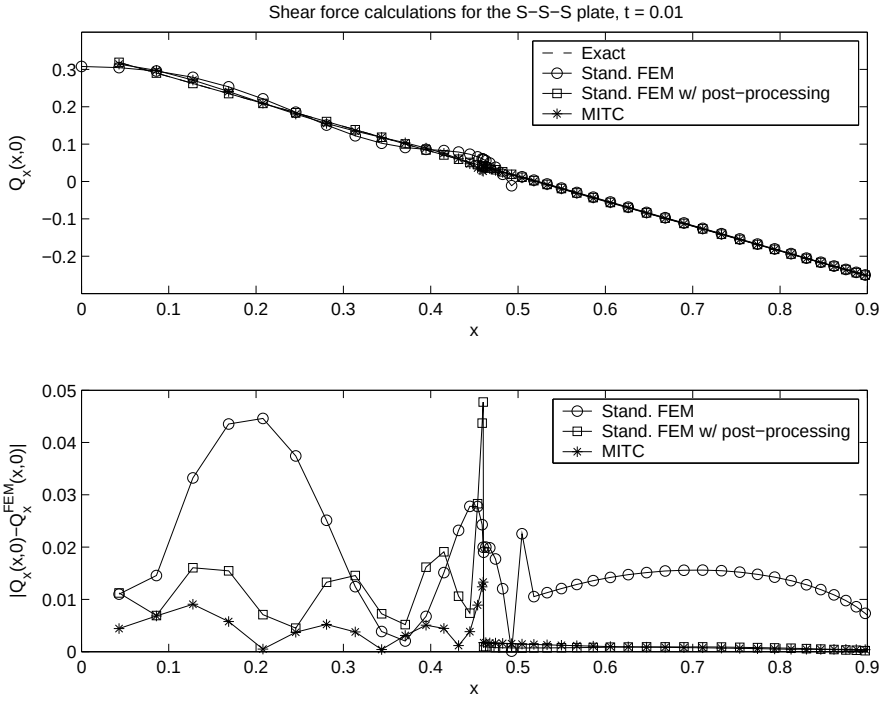

Fig. 13. Shear force computations for the S-S-S plate, $t = 0.01$.

problems, even when curved elements are used, provided that certain care is taken in constructing the element mappings. This information should prove to be quite useful if one is interested in the more difficult *shell* problem, for which the use of curved elements (and MITC formulations) is pivotal [23].

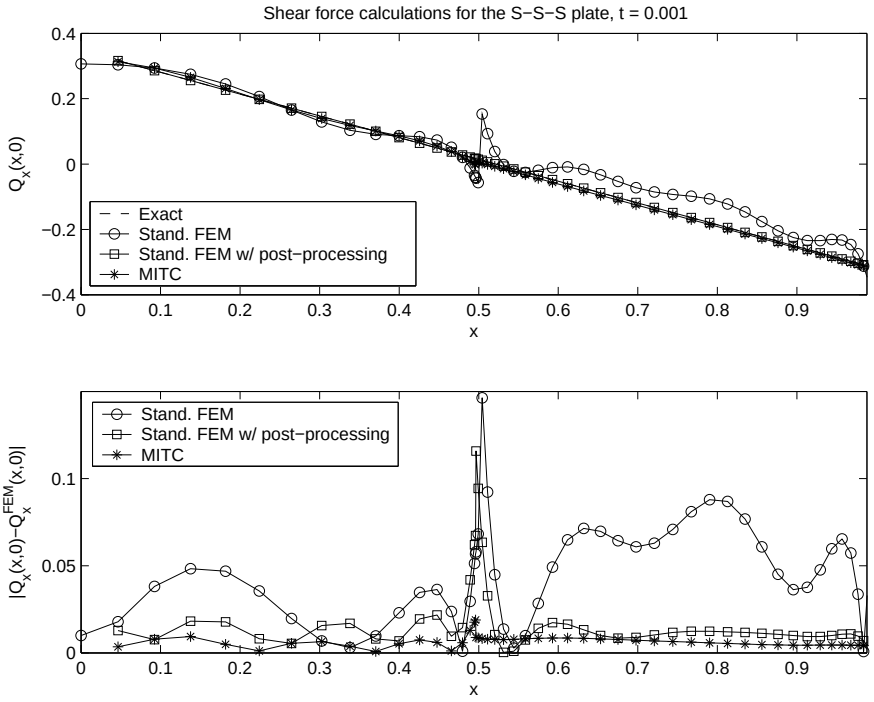

Fig. 14. Shear force computations for the S-S-S plate, $t = 0.001$.

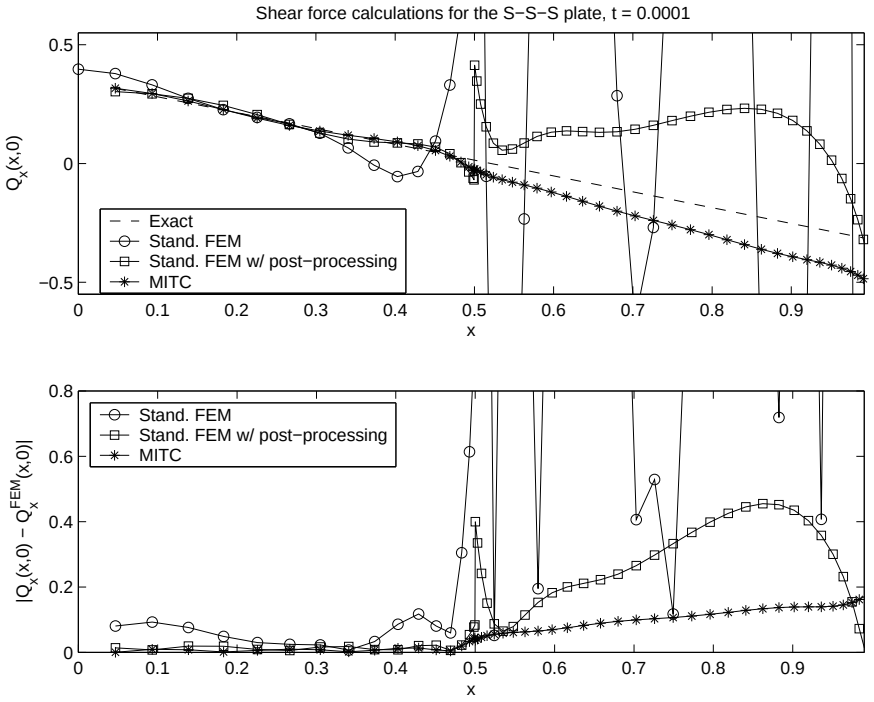

Fig. 15. Shear force computations for the S-S-S plate, $t = 0.0001$.

References

[1] P. A. Raviart and J. M. Thomas, *A mixed finite element method for second order elliptic problems*, *Mathematical Aspects of the Finite Element Method*,

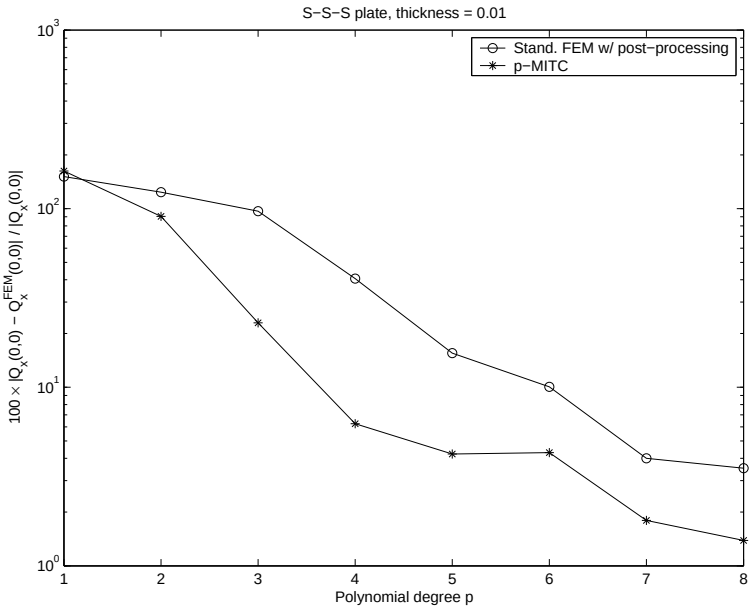

Fig. 16. Convergence of the shear force at (0,0) for the S-S-S plate, $t = 0.01$.

Lecture Notes in Math. 606, Springer-Verlag, NY (1977) 292–315.

[2] F. Brezzi and M. Fortin, *Numerical approximation of Mindlin-Reissner plates*, Math. Comp., 47 (1986) 151–158.

[3] F. Brezzi, J. Douglas Jr., M. Fortin and D. Marini, *Efficient rectangular mixed finite elements in two and three space variables*, RAIRO M^2AN, 21 (1987) 237–250.

[4] D. Arnold and R. Falk, *A uniformly accurate finite element method for the Reissner-Mindlin plate*, SIAM J. Numer. Anal., 26 (1989) 1276–1290.

[5] D. Arnold and R. Falk, *Edge effects in the Reissner-Mindlin plate theory*, *Analytic and Computational Models of Shells*, Noor A K, Belytschko T and Simo J C (eds), A.S.M.E., New York (1989) 71–90.

[6] F. Brezzi, K. J. Bathe and M. Fortin, *Mixed-interpolated elements for Reissner-Mindlin plates*, Int. J. Numer. Meth. Eng., 28 (1989) 1787–1801.

[7] D. Arnold and R. Falk, *The boundary layer for the Reissner-Mindlin plate model*, SIAM J. Math. Anal., 21 (1990) 281–312.

[8] M. Suri, *The p version of the finite element method for elliptic equations of order* 2ℓ, RAIRO M^2AN, 24 (1990) 265–304.

[9] F. Brezzi and M. Fortin, *Mixed and Hybrid Finite Element Methods*, Springer-Verlag, 1991.

[10] F. Brezzi, M. Fortin and R. Stenberg, Error analysis of mixed-interpolated elements for Reissner-Mindlin plates, Mathematical Models and Methods in Applied Sciences, 1 (1991) 125–151.

[11] B. Szabó and I. Babuška, *Finite Element Analysis*, Wiley and Sons, 1991.

[12] P. Peisker and D. Braess, *Uniform convergence of mixed interpolated elements for Reissner-Mindlin plates*, RAIRO M^2AN, 26 (1992) 557–574.

[13] M. Suri and Ch. Schwab, *Locking and boundary layer effects in the finite element approximation of the Reissner-Mindlin plate model*, Proc. Symp. Appl. Math., 48 (1994) 367–371.

[14] M. Suri, I. Babuška and Ch. Schwab, *Locking effects in the finite element approximation of plate models*, Math. Comp., 64 (1995) 461–482.

[15] D. Arnold and R. Falk, *Asymptotic analysis of the boundary layer for the Reissner-Mindlin plate model*, SIAM J. Numer. Anal., 34 (1996) 544–568.

[16] M. Suri, *Analytic and computational assessment of locking in the hp finite element method*, Comput. Methods Appl. Mech. Engrg., 133 (1996) 347–371.

[17] L. K. Chilton, *Locking free mixed hp finite element methods for linear and geometrically nonlinear elasticity*, Ph.D. Dissertation, University of Maryland, Baltimore County, 1997.

[18] R. Stenberg and M. Suri, *An hp error analysis of MITC plate elements*, SIAM J. Numer. Anal., 34 (1997) 544–568.

[19] E. Rank, R. Krausse and K. Preusch, *On the accuracy of p-version elements for the Reissner-Mindlin plate model*, Int. J. Numer. Methods Engrg., 43 (1998) 51-67.

[20] Ch. Schwab, *p- and hp-Finite Element Methods*, Oxford University Press, 1998.

[21] Ch. Schwab, M. Suri and C. Xenophontos, *The hp finite element method for problems in mechanics with boundary layers*, Comput. Methods Appl. Mech. Engrg., 157 (1998) 311–333.

[22] C. Xenophontos, *Finite Element computations for the Reissner-Mindlin plate model*, Comm. Numer. Meth. Engng., 14 (1998) 1119–1131.

[23] K. J. Bathe, A. Iosilevich and D. Chapelle, *An evaluation of the MITC shell elements*, Computers and Structures, 75 (2000) 1–30.

[24] L. Chilton and M. Suri, *On the construction of stable curvilinear p version elements for mixed formulations of elasticity and Stokes flow*, Numer. Math., 86 (2000) 29–48.

[25] J. Kurtz and C. Xenophontos, *On the effects of using curved elements in the approximation of the Reissner-Mindlin plate by the p version of the finite element method*, Applied Numerical Mathematics, 46 (2003) 231–246.

[26] J. Kurtz, *A p version Finite Element Method for Shear Force Computation in Reissner-Mindlin Plates with Curved Boundary*, M.Sc. Thesis, Department of Mathematics and Computer Science, Clarkson University, Potsdam NY, May 2002.

[27] S. Fulton, J. Kurtz and C. Xenophontos, *On the uniform approximation of the Reissner-Mindlin plate model by p/hp finite element methods*, Proceedings of the Fifth World Congress on Computational Mechanics (WCCM V), July 7 - 12, 2002, Vienna, Austria, H. A. Mang, F. G. Rammerstorfer and J. Eberhardsteiner (Eds), ISBN: 3-9501554-0-6.

[28] M. Ainsworth and K. Pichedez, *hp-MITC finite element method for the Reissner-Mindlin plate problem*, Journal of Computational and Applied Mathematics, 148 (2002) 429–462.

[29] M. Ainsworth and K. Pichedez, *hp-Approximation theory for BDFM/RT finite elements and applications*, SIAM J. Numer. Anal., 40 (2002) 2047–2068.